Scientific Research Publishing

Smart Grid and Renewable Energy, 2026, 17(11), 369-389
https://www.scirp.org/journal/sgre
ISSN Online: 2151-4844
ISSN Print: 2151-481X

Integration of Droop Control in Power Flow for Small Rural Islanded Hybrid Microgrids

Tamanjong Fru Fofang[1*], Clinton Kum Ngum[2], Suh Elvice Fru[1]

[1]Department of Renewable Energy, College of Technology, University of Buea, Buea, Cameroon
[2]Department of Electrical and Electronic Engineering, Faculty of Engineering and Technology, University of Buea, Buea, Cameroon
Email: *tamanjong.fofang@ubuea.cm, clinton.ngum93@gmail.com, suh.elvice@ubuea.cm

How to cite this paper: Fofang, T.F., Ngum, C.K. and Fru, S.E. (2026) Integration of Droop Control in Power Flow for Small Rural Islanded Hybrid Microgrids. *Smart Grid and Renewable Energy*, **17**, 369-389.
https://doi.org/10.4236/sgre.2026.1711017

Received: October 21, 2026
Accepted: November 22, 2026
Published: November 25, 2026

Copyright © 2026 by author(s) and Scientific Research Publishing Inc.
This work is licensed under the Creative Commons Attribution International License (CC BY 4.0).
http://creativecommons.org/licenses/by/4.0/

Open Access

Abstract

Electrifying remote and rural communities presents unique challenges, including geographical isolation and low demand. This often makes connection to the main utility grid economically and logistically unfeasible. Islanded hybrid microgrids that integrate renewable energy sources such as solar photovoltaic (PV), small hydropower, biogas-driven generators, and wind with energy storage systems have emerged as a promising, cost-effective solution for off-grid power supply, especially in rural Sub-Saharan communities. However, renewables' inherent intermittency and the lack of a main utility grid to provide frequency and voltage references create significant stability and power-management challenges. This paper investigates droop control as a decentralized strategy to ensure sustainable and reliable operation of a small, rural, islanded hybrid microgrid. Droop control emulates the characteristics of synchronous generators, which is pivotal for enabling parallel operation of multiple inverter-interfaced distributed energy resources (DERs) without high-bandwidth communication links. Motivated by these facts, this study proposes a droop control algorithm for small rural islanded hybrid microgrid systems. To achieve this, we first investigated and identified the root causes of hybrid system design failures in remote and rural communities through field and literature surveys. We then developed a droop-control load-flow algorithm to monitor the steady-state performance of small rural hybrid power systems. The proposed droop-control load-flow algorithm reflects the actual characteristics of small, rural islanded hybrid microgrid operation, where distributed generation units rely on droop control methods. The proposed droop control algorithm is generic and accounts for distribution system features such as feeder and load models. Simulation studies show that with drooping coefficients, mp and nq at 3% and 2%, respectively, the system bus voltages are optimized, with a maximum at bus 5 with a p.u. voltage of 0.963015 and a mini-

mum at bus 3 with a p.u. voltage of 0.92361, which are comparatively higher than other variations of the droop coefficients. The simulation also showed that slightly increasing the line parameters further increased bus voltage drops. This study shows that droop control can effectively manage and maintain voltage limits under load changes and renewable-source variability, ensuring power quality for the community.

Keywords

Hybrid Microgrids, Distributed Generation, Droop Control Algorithm

1. Introduction

Access to reliable, affordable, and sustainable energy is a cornerstone of socio-economic development, yet a significant portion of the global population, particularly in remote and rural areas of developing nations, remains without this essential service [1]. The more energy per capita a country consumes, the more developed it is [1]. This energy deficit perpetuates a cycle of poverty, limits educational and healthcare opportunities, and hinders local economic growth [2]. In response to this pressing challenge, islanded hybrid microgrids have emerged as one of the most suitable and cost-effective solutions for off-grid electrification.

According to the World Energy Outlook 2025 [3], Africa's population is expanding at twice the global average, and energy demand is expected to rise by more than 50% by 2040 under current policies. Yet 600 million Africans still live without electricity, and millions more face chronic outages. Geographical isolation, sparse populations, limited infrastructure, and the prohibitive costs of extending national transmission lines render conventional grid extension economically and logistically unfeasible [4]. Low population density, coupled with low education levels, implies low load density and low revenues. These characteristics hinder investment in Sub-Saharan Africa's rural sector.

2. Hybrid Power Systems

Hybrid power systems integrate multiple renewable energy sources, often complemented by energy storage systems and sometimes generator sets, to form a self-sufficient network [4]. The hybrid nature of these distributed generators is critical for overcoming the inherent intermittency of a single renewable source, thereby enhancing overall system reliability and stability. However, operating a small islanded hybrid microgrid presents unique technical challenges not found in large microgrids or traditional grid-connected systems. Due to the absence of a dominant utility power grid to provide a stable frequency and voltage reference, these isolated networks must manage their own power balance and maintain stability [5].

In addition to this operational challenge, the inverter-interfaced distributed en-

ergy resources (DERs) operating in parallel require an effective control strategy. Droop control is a widely adopted decentralized control technique for this purpose [5]. Droop control emulates the natural behaviour of synchronous generators by establishing a relationship between active power and frequency, and between reactive power and voltage. This allows multiple DERs to share the load proportionally without requiring high-bandwidth, centralized communication links, a crucial advantage for small, rural microgrids where communication infrastructure may be limited or expensive [5].

Despite these advantages, applying conventional droop control in rural hybrid microgrids still presents challenges. Low-voltage distribution networks often exhibit a high resistive-to-inductive (R/X) ratio, creating strong coupling between active and reactive power and undermining the basic premise of conventional droop equations [5]. This can cause voltage/frequency deviations and inaccurate power sharing. Studies show that improper droop settings can lead to significant deviations in system frequency and node voltages, negatively impacting system stability and performance [6].

3. Control Architecture for Islanded Microgrids

Operating an islanded microgrid presents unique technical challenges because it lacks a dominant utility grid to provide stable voltage and a reference frequency. Unlike grid-connected systems where distributed generators can operate as constant power sources, islanded microgrids require special control strategies to maintain power balance and ensure supply quality [7]. Control strategies adopted for microgrid control are broadly classified into the following three structures: centralized, decentralized, and distributed architectures [7]. Centralized control, such as the master-slave method, offers accurate power sharing and near-nominal regulation but relies heavily on high-bandwidth communication infrastructure and presents a single point of failure [7]. This approach is often too expensive and impractical for small rural islanded microgrids where communication infrastructure is limited [7]. In contrast, decentralized control methods, which operate based on local measurements without requiring inter-unit communication, have gained significant popularity [7] [8]. Because they do not require communication, these methods reduce costs, enhance reliability, and enable plug-and-play scalability. These advantages are particularly attractive for rural applications [8]. Among decentralized approaches, droop control is the most widely implemented strategy for coordinating parallel inverter-interfaced DERs in islanded microgrids [6].

4. Load Flow and Droop Control: Principles and Application

4.1. Load Flow

Distributed generation refers to electric power generation supplying loads in their neighbourhood [6]. This uses small-scale generation systems to produce electricity close to customers. In distributed generation, size and location are not the only novelty, as the small-scale generation systems are not centrally dispatched [6]. In

the conventional system, the load flow problem involves computing voltage magnitudes and phase angles at each bus in a power system under balanced steady-state operation [9]. Once these quantities are evaluated, the active and reactive power flows through the system elements, such as interconnecting lines, can be deduced. The outcome of this analysis is generally used to evaluate the steady-state, as well as dynamic, performance of interconnected electric systems [9].

Operating microgrids in islanded mode presents many technical challenges. The core of these technical challenges includes regulating voltage and frequency within standard operating ranges, meeting the real and reactive power requirements of the loads within the island, and ensuring an adequate reserve margin within the microgrid [6]. This reserve margin is typically a function of the load factor, the magnitude of the load, the load variation over time, the reliability requirements of the load, and the availability of the distributed generators [6]. The Load flow analyses are performed to investigate these different technical aspects. Conventional algorithms lack the ability to mimic the operating philosophy of islanded microgrids; hence, specialized methods are employed in load flow modelling of microgrids [6].

The work in [10] elaborates on the various steps to carry out power flow analysis in small and medium-sized power systems using the Newton-Raphson method of load flow analysis. They concluded that the Newton-Raphson method of power flow analysis was faster in terms of convergence speed, but programming is more complex [6] [9]. Applying this system to a small distribution generation network faces a major setback because it cannot monitor changes in system frequency and voltage profile.

The work in [11] focused on the design of a microgrid that consists of a wind turbine, PV, micro turbine, proton-exchange membrane (PEM) fuel cell, main grid, and load buses.

As shown in **Figure 1** [11], the energy sources are connected to the network via an interface unit such as a power electronic device. Power electronic systems affect the quality of the system to which they are connected and require new control arrangements [11] [12]. They used MATLAB and the PowerWorld simulator for the load flow study. Because the system is grid-tied, the grid provides infinite-bus characteristics, stabilizing bus voltages and system frequency. Without the grid, the Microgrid Central Controller (MGCC) controls the Micro-source Controller (MC) and Load Controller (LC) to provide system stability, but this system is costly for a rural community.

4.2. Droop Control Implementation in Distributed Generation Network

Hybrid microgrids need continuous monitoring of their components and surroundings to guarantee efficient energy management [6]. Dedicated sensor network and communication infrastructures are necessary to coordinate the control actions and to broadcast the collected data to the interested partners [6]. In small

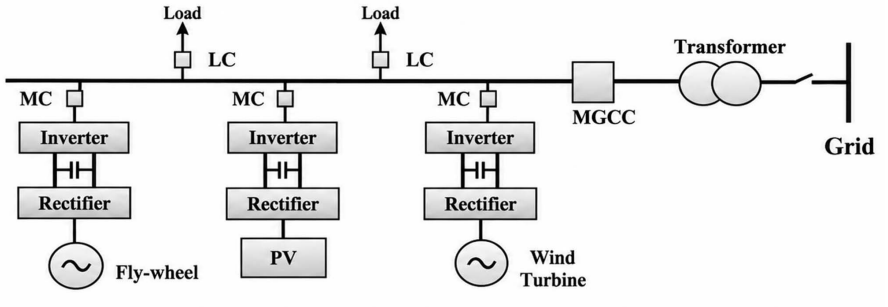


Figure 1. Structure of typical microgrid [11].

rural hybrid microgrids, adding dedicated sensor networks and communication infrastructure increases system cost, making it too expensive for rural communities. An appropriate load flow algorithm can be implemented to act as a communication medium using droop control techniques in small rural hybrid microgrids [13]. In the work in [13], they proposed a hybrid optimization algorithm named "ICGA" based on the imperialist competitive algorithm (ICA) and genetic algorithm (GA) to minimize the total active and reactive power mismatch in the islanded microgrid. This approach is more complex than the Gauss-Seidel algorithm proposed in this work. Microgrids comprise distributed generation sources, storage facilities, and associated loads, which can be grouped as a variety of customers, *i.e.*, residential buildings, commercial units, and industrial parks [14]. In the operation mode, the active and reactive power flow, voltage profile, and frequency must be controlled to achieve reliable electric service [15].

During on-grid operation, the main grid ensures that the microgrid operates within the acceptable frequency and voltage ranges. The main grid absorbs or injects excess/deficit active or reactive power from the microgrid, ensuring a balance between power demand and supply. When the hybrid system is operated in on-grid mode, the system tracks the frequency and phase of the prevailing grid voltage at the point of common coupling PCC [6]. A microgrid connected to the main grid "sees" the latter as a generator with infinite capacity. However, when operated in off-grid mode, the microgrid loses the reference bus at the point of common coupling (PCC) [6]. Therefore, in off-grid mode, the DG units of the microgrid must assume the role of controlling their active and reactive power supply to meet load demand since no slack bus is available anymore [6]. Droop control uses frequency and voltage to control active and reactive power flow, respectively [16].

$$\omega = \omega_0 - m_p P \tag{1}$$

$$V = V_0 - n_p Q \tag{2}$$

where ω_0 and V_0 are the reference angular speed and voltage, respectively. The coefficients m_p and n_q, on the other hand, are the active- and reactive-power static droop gains. These gains specify the frequency or voltage slopes of the droop characteristic of the DG unit [16]. **Figure 2** depicts typical droop control characteristic diagrams.

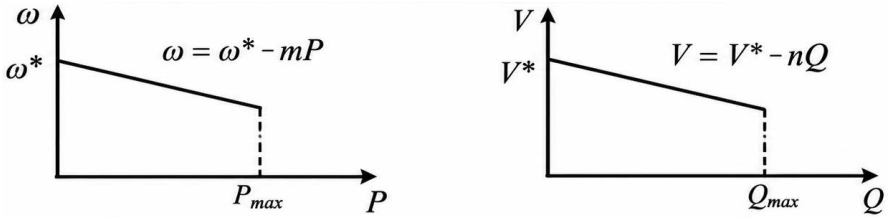


Figure 2. Static droop characteristics [16].

4.3. Including Drooping Characteristics in Load Flow

Distributed generation units are controlled using droop control methods; accordingly, their generated active and reactive powers depend on the power flow variables and are governed by their droop characteristics. Second, system frequency acts as a communication medium between the different DG units in the islanded microgrid; therefore, the steady-state system frequency is not pre-specified and is treated as a power flow variable. The load flow problem is formulated as a set of nonlinear equations that describe power flow in the islanded microgrid system. We propose a convergent Gauss-Seidel method to solve these nonlinear equations. The proposed power flow algorithm, which includes the drooping coefficients, is used to control the small rural hybrid network without implementing communication networks.

5. Methodology Adopted

5.1. Rural Islanded Hybrid System Modelling

5.1.1. Feeder Modelling

In rural islanded hybrid systems, system frequency is a power-flow variable. Therefore, the line reactance model accounts for its variation. The line impedances are converted to admittances.

$$y_{ij} = \frac{1}{Z_{ij}} = \frac{1}{r_{ij} + jx_{ij}} \tag{3}$$

$$Y_{ii} = \sum_{\substack{j=0 \\ j \neq i}}^{n} y_{ij} \tag{4}$$

For a 3-bus rural power system, the bus admittance matrix can be written as:

$$Y_{bus}(\omega) = \begin{bmatrix} Y_{11} & Y_{12} & Y_{13} \\ Y_{21} & Y_{22} & Y_{23} \\ Y_{3}1 & Y_{32} & Y_{33} \end{bmatrix} \tag{5}$$

5.1.2. Load Modelling

The behavior of loads in a rural hybrid power system can be modeled by representing changes in their active and reactive power requirements due to changes in system voltages and frequency. The voltage dependency of load characteristics is represented by the static load models expressed as in [17]

$$P_{Li} = P_{oi} \left| V_i \right|^{K_{pv}} \tag{6}$$

$$Q_{Li} = Q_{oi} \left|V_i\right|^{K_{qv}} \tag{7}$$

where P_{oi} and Q_{oi} are the nominal active and reactive power operating points, respectively; and K_{pv} and K_{qv} are the active- and reactive-power voltage-dependency exponents. In the constant power, constant current, and constant impedance models, the active- and reactive-power voltage-dependency exponents are zero, one, and two, respectively. The values of the active and reactive power voltage dependency exponents for residential, industrial, and commercial loads are given in [17]. The frequency dependency of load characteristics is represented by multiplying the voltage-dependent static load model by a factor as follows [17]:

$$P_{Li} = P_{oi} \left|V_i\right|^{K_{pv}} \left(1 + K_{pf} \Delta\omega\right) \tag{8}$$

$$Q_{Li} = Q_{oi} \left|V_i\right|^{K_{qv}} \left(1 + K_{qf} \Delta\omega\right) \tag{9}$$

where $\Delta\omega$ is the angular frequency deviation ($\omega - \omega_0$); K_{pf} ranges from 0 to 3.0, and K_{qf} ranges from −2.0 to 0 [18]. This work adopts a load-class mix of residential, industrial, and commercial loads to generalize the proposed algorithm and account for load-modeling impacts. **Table 1** shows typically used values for K_{pv} and K_{qv} [18].

Table 1. Typically used values for K_{pv} and K_{qv} [18].

Load Type	K_{pv}	K_{qv}
Constant power	0.00	0.00
Constant Current	1.00	1.00
Residential	0.92	4.04
Commercial	1.51	3.40
Industrial	0.18	6.00

5.1.3. DG Modelling

In grid-connected microgrids, given the relatively small sizes of the DG units, they are controlled as PV or PQ buses. In rural islanded hybrid systems, DG units are operated to share load demands appropriately and to control microgrid voltage magnitude and frequency. Given that there is no slack bus, it will be impossible to make all DG units operate in PV or PQ modes. Accordingly, in islanded microgrids, DG units can operate in three modes: PV, PQ, and droop. For DG units operating in PV mode, the DG units inject a pre-specified quantity of active power and the required reactive power to bring the bus voltage to a pre-specified voltage value. To account for DG reactive current limits, the calculated DG reactive power is compared with the minimum and maximum limits. If the calculated reactive power violates the upper or lower limits, the DG switches from PV to PQ mode, and the reactive power is kept at its limits. When the DG operates in PQ mode, the DG unit injects pre-specified quantities of active and reactive power.

Some of the DG units are interfaced via a power electronic converter and an

output filter [12] [19]. A review of possible converter interface arrangements, different control techniques and synchronization algorithms for DG units can be found in [20]-[22]. **Figure 3** shows the steady-state, fundamental frequency, power flow model of a DG unit operating in droop mode. As shown in **Figure 3**, DG units operating in droop mode, including the energy resource, output filter, and power electronic converter, are modeled as ideal voltage sources whose frequency and voltage magnitude are determined by droop control. This model is sufficient to compute the steady-state operating point for electrical variables at the PCC of each DG unit operating in droop mode, irrespective of the internal power circuit and the control structure used to implement such droop characteristics. For DG units operating in droop mode, the power electronic interface converter, the output filter, the energy resource, and the control structure used to implement the droop characteristics at the PCC of the DG unit do not affect the load flow solution.

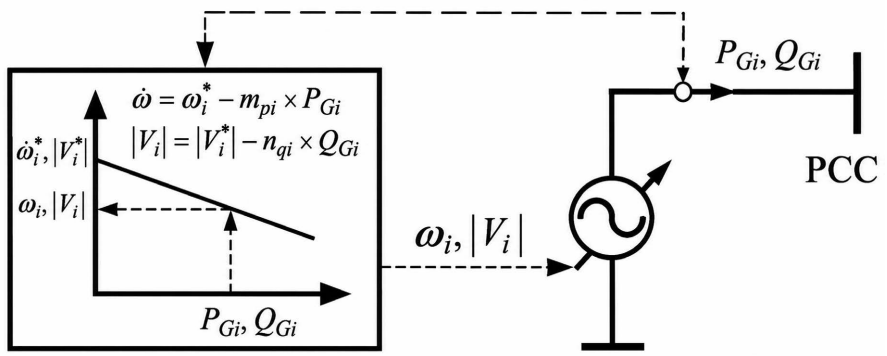


Figure 3. Steady-State, fundamental frequency model of a DG unit operating in droop mode [12].

In the droop mode of operation, active power sharing is realized by introducing droop characteristics to the frequency of the DG unit output voltage at the PCC such that for the DG unit connected to bus *i*:

$$\omega = \omega_i^* - m_{pi} P_{Gi} \tag{10}$$

where ω is the DG output voltage frequency, ω_i^* is the no-load nominal frequency set point, m_{pi} is the active power static droop gain, and P_{Gi} is the injected active power by the DG unit. From Equation (10), it can be seen that the droop characteristic provides a measure of negative feedback that ensures that all the DG units are producing voltages with the same angular frequency at steady state [12].

Reactive power sharing among the different DG units in the hybrid system is achieved by controlling the DG output voltage magnitude. This control is accomplished in a *d-q* frame that rotates with the angular speed ω. A drooping characteristic is introduced in the voltage magnitude of the DG unit output voltage at the PCC such that:

$$V_{di} = V_i^* - n_{qi} Q_{Gi}, \quad V_{qi} = 0 \tag{11}$$

where V_{di} and V_{qi} are the *d*-axis and *q*-axis components of the DG output voltage at bus *i*, respectively, V_i^* stands for the no-load nominal output voltage set point, n_{qi} is the reactive power static droop gain, and Q_{Gi} is the injected reactive power by the DG unit. As per (11), the output voltage magnitude is aligned to the *d*-axis of the DG reference frame, and the output voltage *q*-axis component is set to zero.

The static droop gains for the DG unit connected to bus *i* (m_{pi}, n_{qi}) are conventionally calculated based on the allowable voltage and frequency regulation as well as the DG unit capacity [12].

$$m_{pi} = \frac{\omega^{ub} - \omega^{ib}}{P_{Gi,\max}}, \qquad n_{qi} = \frac{|V_i|^{ub} - |V_i|^{lb}}{Q_{Gi,\max}} \tag{12}$$

where ω^{ub} and ω^{lb} are the upper and lower bounds on system frequency, $|V_i|^{ub}$ and $|V_i|^{lb}$ are the upper and lower bounds on allowable voltage magnitudes at bus *i*, and are the maximum active and reactive power capability of the DG unit. The choice of the minimum and maximum allowable values of the frequency and voltage magnitude depends on the required voltage and frequency regulation [12].

In case of having DG units with different ratings, to achieve proper sharing in proportion to the DG units' ratings, the static droop gains are conventionally chosen as follows:

$$m_{p1}P_{G1,\max} = m_{p2}P_{G2,\max} = \cdots = m_{pi}P_{Gi,\max}, \quad \forall i \in B_{droop} \tag{13}$$

$$n_{q1}Q_{G1,\max} = n_{q2}Q_{G2,\max} = \cdots = n_{qi}Q_{Gi,\max}, \quad \forall i \in B_{droop} \tag{14}$$

where B_{droop} is the set of all droop-controlled buses in the system. Based on (13)-(14), the injected active and reactive power from a DG unit *i* operating with droop control can be expressed in the load flow formulation as follows:

$$P_{Gi} = \frac{1}{m_{pi}}\left(\omega_i^* - \omega\right) \tag{15}$$

$$Q_{Gi} = \frac{1}{n_{qi}}\left(|V_i^*| - |V_i|\right) \tag{16}$$

Typically, the DG units are equipped with a current limiter to limit the production of the DG unit to its rated active and reactive capacities $P_{Gi,\max}$ and $Q_{Gi,\max}$. To incorporate DG current limits into the power flow formulation, the calculated DG active and reactive power generations are compared with their specified limits. If the calculated power violates its limits, the DG switches from droop mode to PQ mode, and the specified power is kept at the limit value.

In this work, we use the conventional droop equations in (15) and (16) in compliance with IEEE 1547.4 for DG islanded systems. These characteristics are usually justified by assuming that the output impedance of the converter is mainly inductive due to the coupling inductor used at the converter output [12], the large inductor of the output filter, or by the use of virtual inductive output impedance [22].

While standards like IEEE 1547 dictate strict trip limits when connected to a bulk utility network, Clause 8.2.7 of IEEE 1547-2018 explicitly allows microgrids to automatically switch to alternative, wider operational settings when operating in islanding mode [23]-[25]. The normal operational range is ±1.0% to ±2.0% of nominal frequency (49.0 - 51.0 Hz for a 50 Hz system). Transient Limits: ±5.0% of nominal frequency (47.5 - 52.5 Hz) [23]-[25].

Voltage profiles in small rural distribution networks are highly sensitive to line length and reactive power balance. The Normal Operational Range is ±5% to ±10% of nominal voltage (0.90 p.u. - 1.10 p.u.) [23]-[25].

5.2. Load Flow Problem Formulation

This section presents the load flow problem formulation in the rural islanded hybrid system. The relation between the branch voltages V_{ij} and branch currents I_{ij} between two nodes *i* and *j* can be expressed as follows:

$$\left|V_{ij}\right| = \left|Z_{ij}\right|\left|I_{ij}\right| \tag{17}$$

The branch currents can be obtained as a function of the branch voltages using

$$\left|I_{ij}\right| = \left|Y_{ij}\right|\left|V_{ij}\right| \tag{18}$$

For each bus *i,* the injected power can be calculated as follows:

$$\left|S_{i,inj}\right| = \left|V_i\right|\left|I_{i,inj}\right|^{conj} \tag{19}$$

where $\left|I_{i,inj}\right|^{conj}$ is the complex conjugate of the injected currents at node *i*. This injected current represents the sum of all the branch currents connected to bus *i*; therefore, the injected current could be given by:

$$\left|I_{i,inj}\right| = \sum_{\substack{j=1 \\ j\neq i}}^{nbus} I_{ij} \tag{20}$$

Let $P_{i,inj}$ and $Q_{i,inj}$ denote the calculated active and reactive power injected to the hybrid system at each bus *i*. The bus current in terms of voltage and apparent power is:

$$I_{i,inj} = \frac{S_i^{conj}}{V_i^{conj}} = \frac{P_{i,inj} - Q_{i,inj}}{V_i^{conj}} \tag{21}$$

$$\frac{P_{i,inj} - Q_{i,inj}}{V_i^{conj}} = \sum_{j=1}^{n} Y_{ij} V_j \tag{22}$$

$$P_{i,inj} - Q_{i,inj} = V_i^{conj} \sum_{j=1}^{n} Y_{ij} V_j = V_i \sum_{j=1}^{n} Y_{ij}^{conj} V_j^{conj} \tag{23}$$

By equating the real and imaginary terms of the above expression, we derive two equations for each bus in terms of four variables: *P*, *Q*, *V*, and the angle *θ*. The above equations for active and reactive power are solved using the Gauss-Seidel numerical method.

5.3. Application of Gauss-Seidel to Microgrid Load Flow Problems

The load flow problem in a standalone hybrid microgrid is characterized by the following salient features:

- There is no slack bus
- The system frequency is not constant
- The Y_{bus} matrix varies with the fluctuation of the frequency
- The line losses are not constant due to the variation in system voltages and frequency

To minimize divergence problems of the modified load flow algorithm, initial guesses of voltage and angle magnitudes are first calculated using the conventional load flow algorithm. These initial guesses are then fed to the modified load flow algorithm.

5.3.1. Calculation of the Voltage at All Buses and the System Losses

The voltage at all buses is calculated using the following expression:

$$V_{ii}^{k+1} = \frac{1}{Y_{ii}}\left[\frac{P_i - jQ_i}{\left(V_i^k\right)^*} - \sum_{n=1}^{i-1}\left(Y_{in}V_n^{k+1}\right) - \sum_{n=i+1}^{N}\left(Y_{in}V_n^k\right)\right] \tag{24}$$

where V_i^{k+1} = Voltage for iteration $(k+1)$ at bus i

Equation (24) gives both voltage magnitude and angle for the current iteration. The algorithm requires selecting a reference bus. When the voltage is calculated for the selected reference bus, the resulting magnitude from Equation (24) is kept, while the angle is reset to zero. For droop-controlled buses, P_i and Q_i are estimated using Equations (19) and (20), respectively. For all PQ or load buses, P_i and Q_i are constant and readily known through Equations (22) and (23). For PV buses, active power and bus voltage are constant and preselected. The reactive power is evaluated using the following expression:

$$Q_i^{k+1} = -\mathrm{Im}\left[\left(V_i^k\right)^*\left(\sum_{n=1}^{i-1}\left(Y_{in}V_n^{k+1}\right) - \sum_{n=i}^{N}\left(Y_{in}V_n^k\right)\right)\right] \tag{25}$$

Once the reactive power generated at a PV bus is calculated, it must be verified to be within the *unit's Q limits*. If the calculated value exceeds the maximum boundary, set it to Q_{max}. Second, when the voltage at the PV bus is calculated, the new bus angle is kept, while the magnitude is reset to its predefined value. Droop equations are used to evaluate the active and reactive power output at VF buses.

5.3.2. Calculation of the New System Frequency

Assuming all DGs in the islanded microgrid operate droop-based, the sum of active power generated by the DGs equals the total power circulating within the microgrid. Since the frequency is the same throughout the microgrid, droop-controlled buses supply active power at the same angular frequency. Bidirectional converters are used to interface between DG units. Considering these observations, the following expression can be written:

$$P_{total} = P_{load} + P_{line_losses} = \sum_{i=1}^{d} P_{Gi} = \sum_{i=1}^{d} \frac{1}{m_{pi}} (\omega_0 - \omega) \tag{26}$$

From Equation (26), the system frequency can be derived as follows:

$$\omega^{k+1} = \frac{\sum_{i=1}^{d} \frac{1}{m_{pi}} \omega_0 - \left(P_{load}^{k+1} + P_{line_loss}^{k+1}\right)}{\sum_{i=1}^{d} \frac{1}{m_{pi}}} \tag{27}$$

where d denotes droop-controlled generators.

5.3.3. Calculation of the Generated Reactive Power

The generated reactive power is evaluated and compared to the reactive power consumed by the loads. The total reactive power generated by droop-controlled generators can be derived from the expression relating the generated reactive power due to voltage mismatch, $V_{ref} - V_i$, and the voltage droop coefficient, n_q. The reactive power generated at PV buses is calculated as shown in the previous section. To ensure that the reactive power demand of the system is met, the calculated new voltages must satisfy the following expression:

$$Q_{system} = \sum_{i=1}^{g} Q_{Gi} + Q_{PV} = \sum_{i=1}^{g} \frac{1}{n_{qi}} (V_0 - V_i) + Q_{PV} \tag{28}$$

Once the new frequency is evaluated, the new admittance matrix is re-calculated, and the process is repeated to get the new bus voltages. The process is repeated until the error between the new $(k+1)$ and the old (k) values of the voltages and the angular frequency is less than the pre-defined error margin. The mismatch between generated and consumed reactive power must also be less than the error margin. Figure 4 depicts a flowchart that shows the steps involved in the integrated droop-control load flow algorithm.

As shown in the flowchart of Figure 4, the initial guesses of the unknown variables are calculated using the conventional load flow algorithm. This is to improve convergence. The initial values are then fed to the integrated droop-control algorithm. In running the conventional load flow algorithm, all droop-controlled generators are assumed to be operated in PV mode.

6. Results

Droop Control and Load Flow Algorithm Validation

To validate the applicability of the droop-control load flow algorithm, a balanced 6-bus test system shown in Figure 5 was used. We chose this system because it is small, balanced, and representative of a small rural hybrid system. This system includes three identical droop-based DG units and represents an islanded hybrid system. Tables 2-4 show the distributed generator ratings, line parameters, and load parameters, respectively.

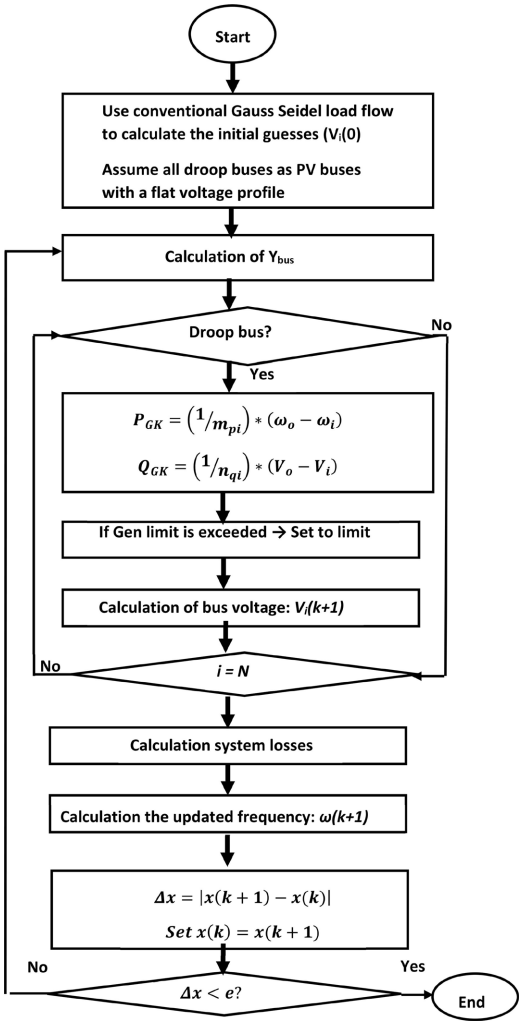


Figure 4. Flowchart of the integrated droop-control load flow algorithm.

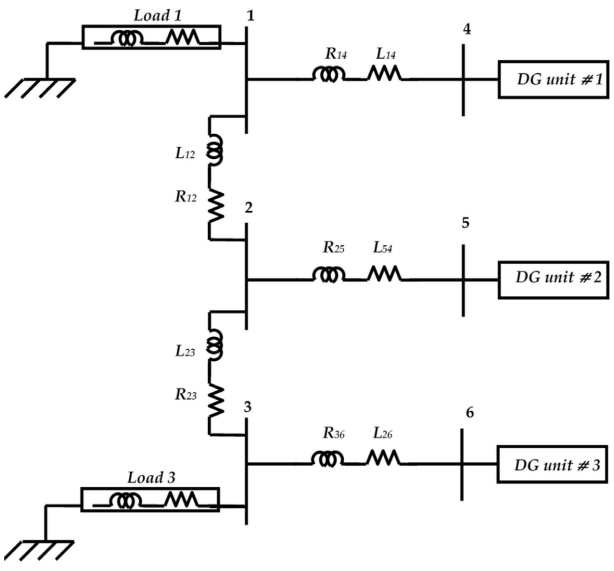


Figure 5. Single-Line diagram of the 6-bus microgrid test system.

Table 2. DG ratings.

S, kVA	5
P, kW	4
Q, kVAR	3
S_{base}, kVA	**1**
V_{base}, V (phase-phase)	**220**
Z_{base}, Ω	**48.4**
f, Hz	**50**
Frequency droop, ($P-f$)%	**0.5 - 5**
Voltage droop, ($Q-V$)%	**1 - 5**
Droop Gain, p.u.	**0.01 - 0.05**

Table 3. Line parameters of the six-bus microgrid.

Line Parameters (per phase)			
From bus	To bus	R_{line}	L_{line}
1	2	0.43	0.318
2	3	0.15	1.843
3	6	0.05	0.050
4	1	0.30	0.530
2	5	0.28	0.250

Table 4. Load parameters.

System Load (per phase) Load p.f., 0.8 lag		
Bus Number	Load Resistance (ohm)	Line Ind. (mH)
1	6.95	12.2
2	0	0
3	5.014	9.4
4	0	0
5	0	0
6	0	0

Figure 6 shows the bus voltage plot. The plot shows that voltages at the generation buses are much higher than those at the load buses due to line losses.

It was also observed that the interconnecting bus (bus number 2) has a higher voltage than the load buses 1 and 3.

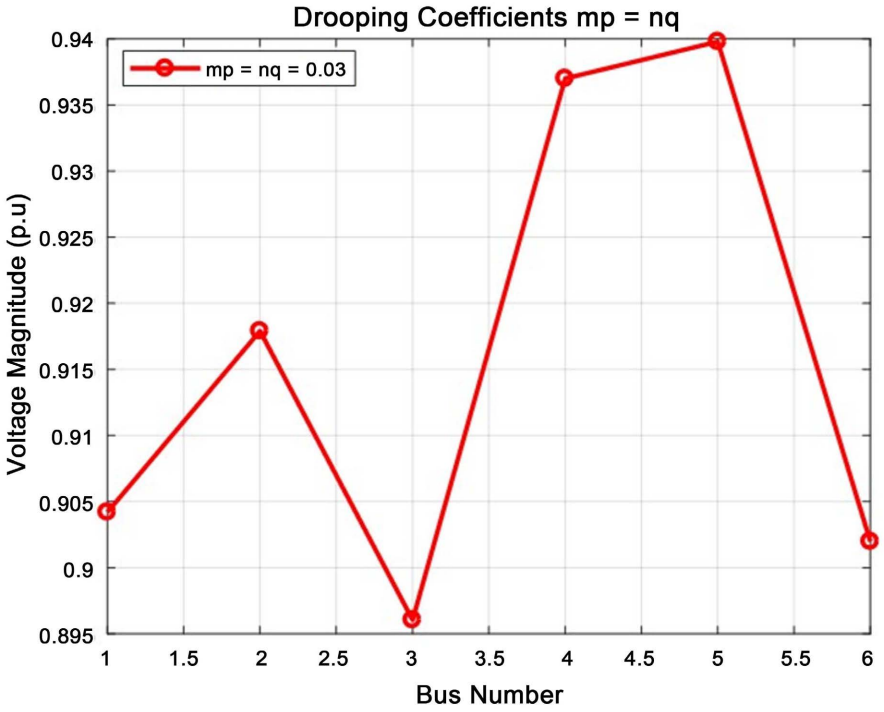
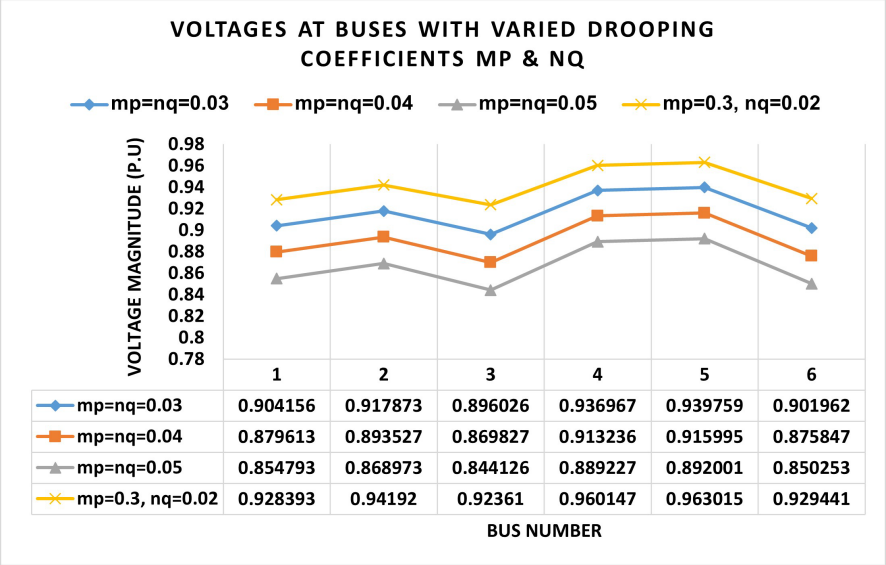


Figure 6. Bus voltages with rated droop settings.



	1	2	3	4	5	6
mp=nq=0.03	0.904156	0.917873	0.896026	0.936967	0.939759	0.901962
mp=nq=0.04	0.879613	0.893527	0.869827	0.913236	0.915995	0.875847
mp=nq=0.05	0.854793	0.868973	0.844126	0.889227	0.892001	0.850253
mp=0.3, nq=0.02	0.928393	0.94192	0.92361	0.960147	0.963015	0.929441

Figure 7. Voltages at buses with varied droop coefficients.

Figure 7 shows that changes in droop control produce corresponding changes in frequency and voltage at the droop-controlled buses. To capture the effects of changes in the operating-state frequency and voltage, the speed droop control (active power static droop control m_p) and the voltage droop control (reactive power static droop control n_q) of all three droop-controlled distributed generation units are varied. These changes depict the effect of using distributed generation resources with different droop characteristics.

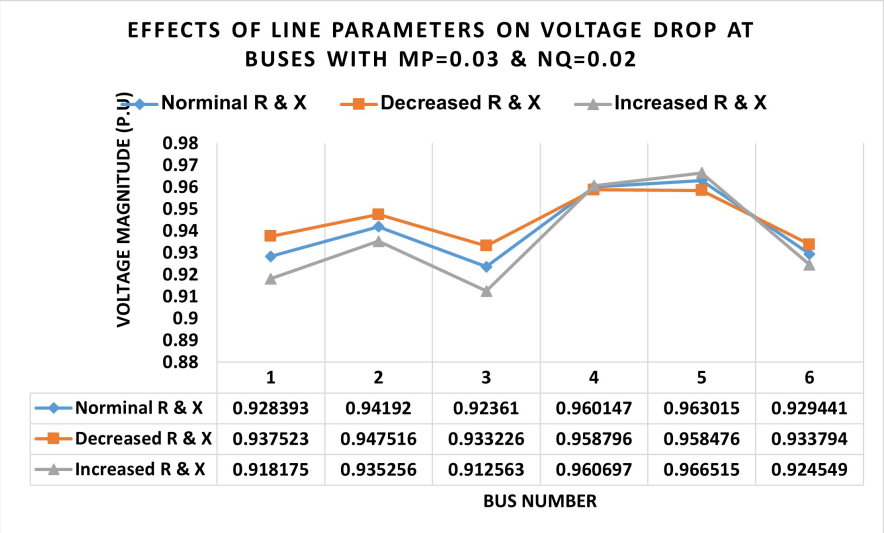


Figure 8. Effects of changes in line parameters on voltage drop at buses with m_P set at 3% and n_P at 2%.

The effects of line parameters on voltage drop at PQ buses for given m_P and nq set points are verified as shown in Figures 8-11. The results confirm that the voltage drop increases with higher line parameters and drooping coefficients.

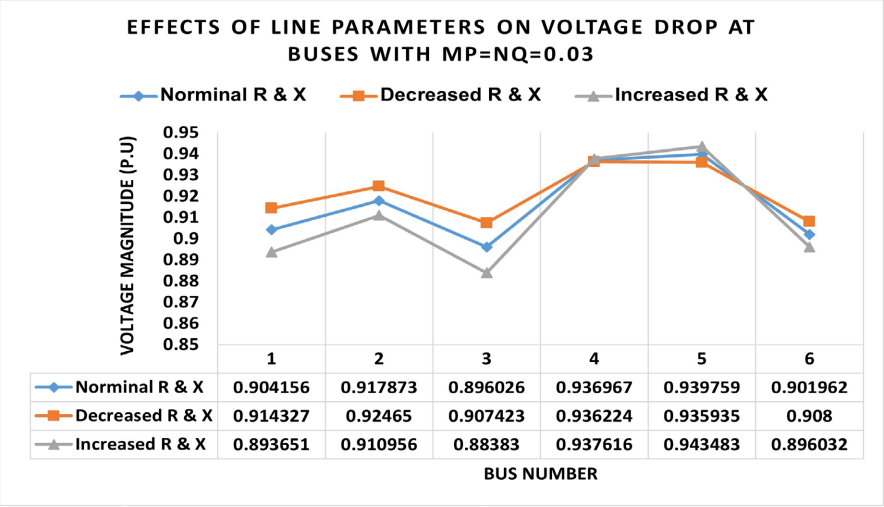
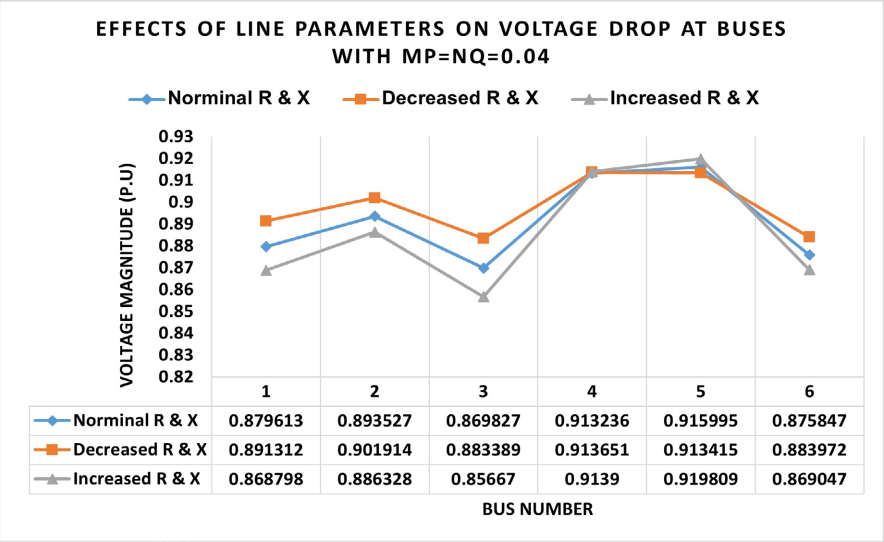


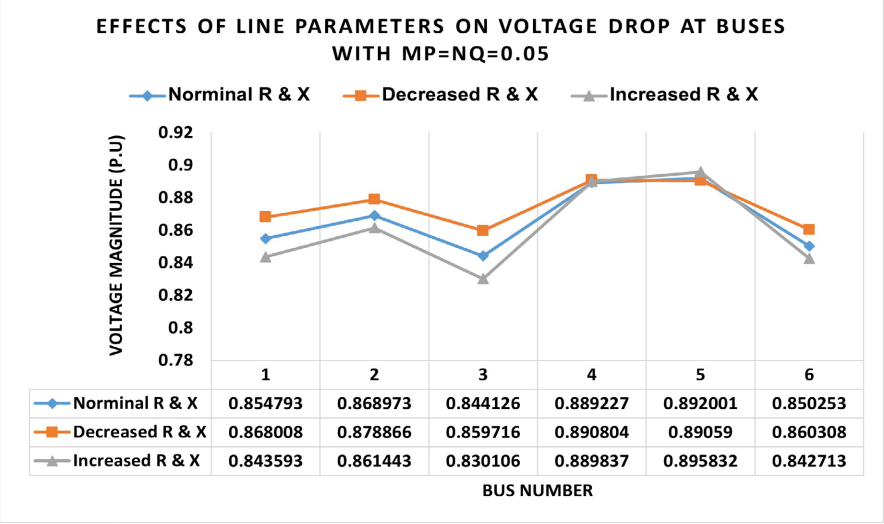
Figure 9. Effects of changes in line parameters on voltage drop at buses with $m_P = n_P = 3\%$.

The frequency regulation performance of droop control in load flow was evaluated under varying load conditions. Results from the droop-control implementations showed that frequency deviations remained within acceptable bounds for most operating conditions. However, the approach showed limitations in steady-state frequency accuracy, though they were insignificant enough not to affect steady-state load performance. The system frequency was fairly constant between no-load and full load, as shown in Figure 12. As seen in Figure 13, the frequency variation between no-load and full load is 0.9 Hz.



	1	2	3	4	5	6
Norminal R & X	0.879613	0.893527	0.869827	0.913236	0.915995	0.875847
Decreased R & X	0.891312	0.901914	0.883389	0.913651	0.913415	0.883972
Increased R & X	0.868798	0.886328	0.85667	0.9139	0.919809	0.869047

Figure 10. Effects of changes in line parameters on voltage drop at buses with $m_p = n_p$ at 4%.



	1	2	3	4	5	6
Norminal R & X	0.854793	0.868973	0.844126	0.889227	0.892001	0.850253
Decreased R & X	0.868008	0.878866	0.859716	0.890804	0.89059	0.860308
Increased R & X	0.843593	0.861443	0.830106	0.889837	0.895832	0.842713

Figure 11. Effects of changes in line parameters on voltage drop at buses with $m_p = n_p = 5\%$.

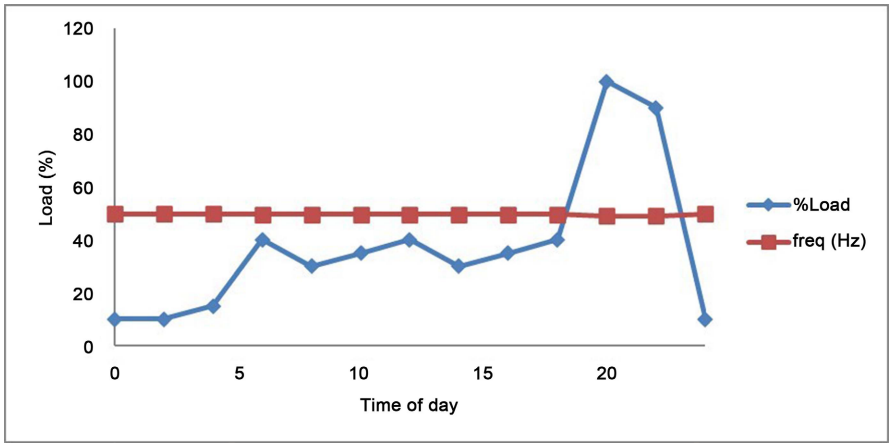


Figure 12. Load and frequency variation.

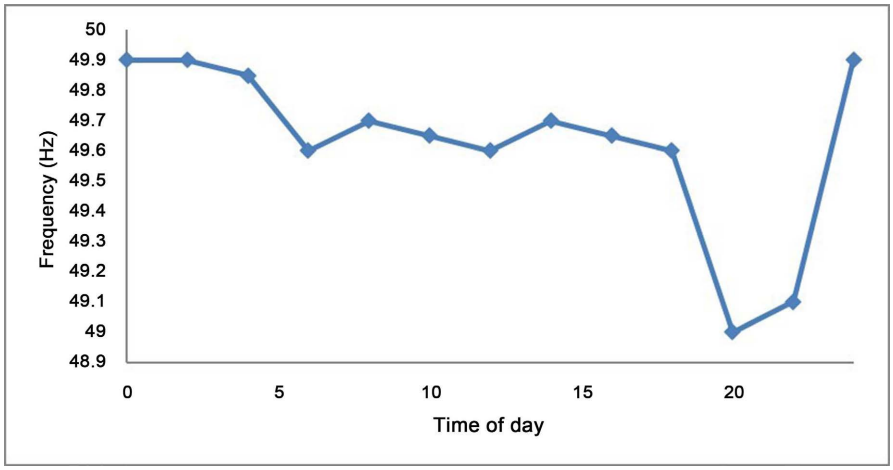


Figure 13. Frequency variation between no-load and full load.

7. Discussion

This section presents the simulation results evaluating the performance of the droop control strategy applied to a small rural islanded hybrid microgrid. The analysis focuses on two key performance criteria: voltage and frequency regulation and power-sharing accuracy among distributed energy resources (DERs). The results demonstrate the effectiveness of conventional droop control in small rural islanded hybrid microgrids. The study evaluated droop control's power-sharing capabilities under full-load and generation conditions. The droop control achieved acceptable power sharing among parallel-connected DERs. However, it avoided significant impedance mismatch, a common issue in rural low-voltage networks with varying feeder lengths and conductor sizes, where power-sharing accuracy degrades significantly. The results also reinforce the importance of a hierarchical control architecture for larger islanded microgrid operation, where primary-level droop control provides the first line of defense for system stability through decentralized, communication-free power sharing. The secondary and tertiary control levels, responsible for voltage/frequency restoration and economic dispatch, respectively, can be implemented with varying degrees of communication dependence based on available infrastructure.

8. Conclusion

8.1. Summary of Contributions

This paper investigated integrating droop control into power flow for small rural islanded hybrid microgrids, addressing both theoretical foundations and practical implementation considerations. The study provides quantitative evidence that droop control effectively maintains voltage and frequency limits in rural islanded microgrids. Based on this comprehensive analysis, droop control is a robust, scalable, communication-free decentralized control strategy well suited to small rural islanded hybrid microgrids. Its simplicity, reliability, and low implementation cost make it particularly advantageous for resource-constrained rural settings.

Again, droop-controlled hybrid microgrids are economically viable, with positive financial metrics and meaningful sustainability benefits, supporting their role as a key solution for rural electrification in developing regions.

8.2. Limitations and Future Research

The results show that conventional droop control exhibits some limitations when applied to small rural islanded microgrids. The primary challenge stems from the nature of low-voltage distribution networks common in rural areas, which typically exhibit a high resistive-to-inductive (R/X) ratio. In such networks, the integrated droop control's assumption of decoupling between active and reactive power breaks down, creating strong coupling between these quantities. This coupling leads to inaccuracies in power sharing and significant voltage and frequency deviations. The choice of droop gains becomes a critical trade-off: high droop gains can improve power-sharing accuracy but may destabilize the system, while low gains ensure stability but lead to poor load sharing and larger frequency deviations. The intermittent nature of renewable sources further compounds these issues, as variable generation requires droop settings that can adapt to changing operating conditions. These limitations require further research into enhanced droop control strategies for small rural hybrid microgrids. However, as research advances, intelligent control techniques, validation methods, and implementation frameworks, droop control will remain a cornerstone technology for rural electrification, contributing to a more equitable and sustainable energy future.

Author Contributions

Tamanjong Fru Fofang contributed to the study conception, design, writing, and funding. All authors contributed to the material preparation, data collection, analysis, review, and editing of the manuscript.

Conflicts of Interest

The authors declare no conflicts of interest regarding the publication of this paper.

References

[1] Sorif, S.M., Das, S.K. and Sarkar, S. (2025) Optimal Allocation and Droop Setting of Droop-Controlled Distributed Generations for Effective Operation of Islanded Microgrid with Solar PV and Wind Generator. 2025 *Fourth International Conference on Power, Control and Computing Technologies* (ICPC2T), Raipur, 20-22 January 2025, 68-73. https://doi.org/10.1109/icpc2t63847.2025.10958590

[2] Nforngwa, E.N. and Fulai, U.M. (2024) Scaling up Renewable Energy to Improve Electricity Access in Cameroon: Policy Pathways. https://www.acsea54.org/wp-content/uploads/2024/09/policy-brief-scaling-RE-access-in-Cameroon-acsea-assigment-.pdf

[3] International Energy Agency (2019) World Energy Outlook 2019. International Energy Agency.

[4] Makai, L. and Popoola, O. (2025) A Review of Micro-Hybrid Energy Systems for Ru-

ral Electrification, Challenges and Probable Interventions. *Renewable Energy Focus*, **53**, Article 100687. https://doi.org/10.1016/j.ref.2025.100687

[5] Hossain, M.I., Anonto, H.Z., Rohan, A.I., Shufian, A. and Ghosh, D.K. (2025) Optimizing Power Distribution and Stability in Islanded Microgrids with Wind Energy Integration Using Enhanced Droop and Virtual Impedance Control. *Results in Engineering*, **27**, Article 106970. https://doi.org/10.1016/j.rineng.2025.106970

[6] Zambroni, C.A. and Castilla, M. (2019) Microgrids Design and Implementation. Springer.

[7] Kreishan, M.Z. and Zobaa, A.F. (2021) Optimal Allocation and Operation of Droop-Controlled Islanded Microgrids: A Review. *Energies*, **14**, Article 4653. https://doi.org/10.3390/en14154653

[8] Oladigbolu, J.O., Ramli, M.A.M. and Al-Turki, Y.A. (2020) Optimal Design of a Hybrid PV Solar/Micro-Hydro/Diesel/Battery Energy System for a Remote Rural Village under Tropical Climate Conditions. *Electronics*, **9**, Article 1491. https://doi.org/10.3390/electronics9091491

[9] Das, D. (2006) Electrical Power Systems. New Age International Ltd.

[10] Lakshmi, P.Y. (2016) Power Flow Analysis of Integrated Wind and Solar Power Generation and Distribution System. *International Journal of Engineering Research & Technology* (IJERT), **5**, 214-216.

[11] Nur, A. and Kaygusuz, A. (2016) Power Flow Study for a Microgrid by Using Matlab and Powerworld Simulator. *International Journal of Energy and Smart Grid*, **1**, 14-21. https://doi.org/10.23884/ijesg.2016.1.1.02

[12] Pogaku, N., Prodanovic, M. and Green, T.C. (2007) Modeling, Analysis and Testing of Autonomous Operation of an Inverter-Based Microgrid. *IEEE Transactions on Power Electronics*, **22**, 613-625. https://doi.org/10.1109/tpel.2006.890003

[13] Abedini, M. (2016) A New Algorithm for Load Flow Analysis in Autonomous Networks. *International Journal of Smart Electrical Engineering*, **5**, 176-182.

[14] Lidula, N.W.A. and Rajapakse, A.D. (2011) Microgrids Research: A Review of Experimental Microgrids and Test Systems. *Renewable and Sustainable Energy Reviews*, **15**, 186-202. https://doi.org/10.1016/j.rser.2010.09.041

[15] Rocabert, J., Luna, A., Blaabjerg, F. and Rodríguez, P. (2012) Control of Power Converters in AC Microgrids. *IEEE Transactions on Power Electronics*, **27**, 4734-4749. https://doi.org/10.1109/tpel.2012.2199334

[16] Chapman, S.J. (1999) Electric Machinery Fundamentals. McGraw Hill.

[17] IEEE (1995) Bibliography on Load Models for Power Flow and Dynamic Performance Simulation. *IEEE Transactions on Power Systems*, **10**, 523-538.

[18] Kundur, P. (1994) Power System Loads in Power System Stability and Control. McGraw-Hill.

[19] Blaabjerg, F., Chen, Z. and Kjaer, S.B. (2004) Power Electronics as Efficient Interface in Dispersed Power Generation Systems. *IEEE Transactions on Power Electronics*, **19**, 1184-1194. https://doi.org/10.1109/tpel.2004.833453

[20] Prodanovic, M., Green, T. and Mansir, H. (2000) A Survey of Control Methods for Three-Phase Inverters in Parallel Connection. 8*th International Conference on Power Electronics and Variable Speed Drives*, London, 18-19 September 2000, 472-477.

[21] Green, T.C. and Prodanović, M. (2007) Control of Inverter-Based Micro-Grids. *Electric Power Systems Research*, **77**, 1204-1213. https://doi.org/10.1016/j.epsr.2006.08.017

[22] Guerrero, J.M., GarciadeVicuna, L., Matas, J., Castilla, M. and Miret, J. (2005) Output Impedance Design of Parallel-Connected UPS Inverters with Wireless Load-Sharing Control. *IEEE Transactions on Industrial Electronics*, **52**, 1126-1135. https://doi.org/10.1109/tie.2005.851634

[23] Kumar, J., Agarwal, A. and Agarwal, V. (2019) A Review on Overall Control of DC Microgrids. *Journal of Energy Storage*, **21**, 113-138. https://doi.org/10.1016/j.est.2018.11.013

[24] Mahmoud, M.S. and Alyazidi, N.M. (2017) Advanced Control Methods and Renewable Energy System Integration. Butterworth-Heinemann.

[25] Mohamad, H., Mokhlis, H., Bakar, A.H.A. and Ping, H.W. (2011) A Review on Islanding Operation and Control for Distribution Network Connected with Small Hydro Power Plant. *Renewable and Sustainable Energy Reviews*, **15**, 3952-3962. https://doi.org/10.1016/j.rser.2011.06.010